https://doi.org/10.5194/essd-2025-497
Preprint. Discussion started: 13 October 2025

An improved GRACE-derived groundwater storage anomaly (igGWSA) dataset over global land with full consideration of non-groundwater components based on current new datasets

Zongxia Wang[a, b], Suxia Liu[a, b, c], Xingguo Mo[a, b, c]

[a] *Key Laboratory of Water Cycle and Related Land Surface Processes, Institute of Geographic Sciences and Natural Resources Research, Chinese Academy of Sciences, Beijing 100101, China*

[b] *College of Resources and Environment, University of Chinese Academy of Sciences, Beijing 100049, China*

[c] *Sino-Danish College, University of Chinese Academy of Sciences, Beijing 100049, China*

Correspondence to: Suxia Liu (liusx@igsnrr.ac.cn)

Abstract: Accurate quantification of global groundwater storage anomaly (GWSA) is imperative for global water security and socio-economic sustainability. The Gravity Recovery and Climate Experiment (GRACE) satellite has emerged as a prevailing methodology for estimating GWSA. However, oversimplification of non-groundwater components potentially compromised its accuracy in most previous studies. Here we present an improved GRACE-derived GWSA dataset at the global scale, namely igGWSA, with full consideration of non-groundwater components including glaciers, snow, permafrost, lakes, reservoirs, surface runoff, profile soil moisture (PSM), and plant canopy water based on current new datasets. In particular, PSM was generated based on Catchment Land Surface Model and random forest algorithm. igGWSA demonstrated strong agreement with well-observed groundwater level and model-simulated GWSA in five globally recognized hotspots of groundwater depletion. Compared to igGWSA with full consideration, simplified estimation would lead to misinterpretations of groundwater storage variations in glacier-covered regions, giant lakes, and deep-soil areas, highlighting the necessity of comprehensively accounting for non-groundwater components in estimating GWSA, especially under a changing environment. igGWSA dataset is publicly available on Zenodo through https://doi.org/10.5281/zenodo.16871689 (Wang et al., 2025).

https://doi.org/10.5194/essd-2025-497
Preprint. Discussion started: 13 October 2025

Open Access Earth System Science Data Discussions

1. Introduction

Constituting the Earth's largest reservoir of liquid freshwater, groundwater serves as a critical hydrological component in global terrestrial water cycle (Adams et al., 2022). Groundwater is a fundamental source of drinking water and agricultural irrigation, with 38% of global area equipped for irrigation relying on groundwater (Siebert et al., 2010). Groundwater-dependent ecosystems (GDEs) are identified worldwide (Link et al., 2023) and are found to be closely associated with biodiversity hotspots across global drylands (Rohde et al., 2024). Therefore, groundwater is of great significance for achieving the sustainable development goals (SDGs) proposed by the United Nations, such as No Poverty (SDG 1), Zero Hunger (SDG 2), Clean Water and Sanitation (SDG 6), Climate Action (SDG 13), and Life on Land (SDG 15) (Gleeson et al., 2020). However, climate change has imposed profound impacts on the atmosphere, hydrosphere and cryosphere (Prein and Heymsfield, 2020; Su et al., 2022; Ombadi et al., 2023), and particularly triggered changes in groundwater storage (GWS) through altering water supply-demand balance and groundwater recharge (Taylor et al., 2013; Condon et al., 2020; Kuang et al., 2024). Moreover, intensified anthropogenic activities (e.g., groundwater withdrawals for irrigation) have led to global groundwater depletion (Wada et al., 2010; De Graaf et al., 2017), which left vast populations threatened by unsustainable groundwater resources (Gleeson et al., 2012) and gave rise to eco-environmental issues such as land subsidence (Hasan et al., 2023) and river baseflow reduction (De Graaf et al., 2024). Therefore, accurate and quantitative monitoring of GWS variations is essential for ensuring global water security, food security, and socio-economic sustainability.

Conventional monitoring of groundwater dynamics primarily depends on well-based observations. Despite the high reliability, the availability of such data remains severely constrained by economic costs, spatial accessibility, and data sharing policies (Adams et al., 2022). Consequently, related studies are typically conducted at local to regional scales, whereas large-scale and particularly global-scale analyses remain critically underexplored (Fan et al., 2013; Berghuijs et al., 2022; Jasechko et al., 2024). Notably, all these few large-scale studies suffer from spatial underrepresentation due to the extremely uneven distribution of monitoring wells. Moreover, point-scale measurements fail to delineate spatially continuous groundwater dynamics, nor can they adequately capture the heterogeneity of

https://doi.org/10.5194/essd-2025-497
Preprint. Discussion started: 13 October 2025

hydrogeological characteristics. Hydrological models provide an alternative approach to address the spatial limitations of in situ observations. Nevertheless, the reliability of model-simulated groundwater dynamics is subject to other limitations. For example, the accuracy of simulations is sensitive to quality of forcing data and inherent uncertainties in model structure (Döll and Fiedler, 2008; Berghuijs et al., 2022). Besides, owing to the absence of human activity module, many models capture only natural variability patterns without accounting for the effects of human-induced hydrological processes such as groundwater abstraction and irrigation practices (Fan et al., 2013; Pokhrel et al., 2021). In addition, the vertical representation of aquifer systems in some models is too simplified to reliably simulate the evolution of GWS (Gascoin et al., 2009).

In 2002, the Gravity Recovery and Climate Experiment (GRACE) satellite was launched jointly by the National Aeronautics and Space Administration (NASA) and Deutsches Zentrum für Luft- und Raumfahrt (DLR) (Tapley et al., 2004a). GRACE mission has created unprecedented opportunities for detecting terrestrial mass redistribution and provided an innovative perspective to quantify GWS variations (Tapley et al., 2004b). Changes in GWS can be isolated from changes in GRACE-detected terrestrial water storage (TWS) by removing other non-groundwater components (Rodell et al., 2009). Compared to in situ observations and model simulations, GRACE-based estimation demonstrates distinct superiority. Horizontally, the global coverage of GRACE enables continuous monitoring of large-scale groundwater variations. Vertically, GRACE-derived groundwater storage anomaly (GWSA) represents the integrated dynamics of aquifer systems, providing more holistic characterization than monitoring wells or predictions of hydrological models.

Although GRACE has emerged as a prevailing methodology for GWS estimation, limitations still remain in current GRACE-based studies. On the one hand, TWS is the summation of GWS and non-groundwater storage. The more comprehensively non-groundwater components are taken into account, the more accurate the separated GWS information will be. However, non-groundwater components considered in most previous studies only encompass soil moisture, snow, plant canopy water, and surface runoff (Table S1), which may be applicable to areas with limited types of water bodies. For areas characterized by complicated hydrological systems (e.g., coexisting glaciers, permafrost, and lakes), such ignorance will erroneously attribute the signals of unaccounted

https://doi.org/10.5194/essd-2025-497
Preprint. Discussion started: 13 October 2025

components to changes in GWS, which will consequently compromise the accuracy of GWSA estimation. Among the neglected components, glaciers typically exhibit the most pronounced magnitude of mass change. Therefore, the potential impact of incomprehensive consideration on GWSA estimation is expected to be the greatest in glacier-covered regions. Due to the absence of glacier module in most land surface models (LSMs) and hydrological models, glacier mass balance cannot be obtained from model simulations as other components. To our knowledge, the vast majority of previous studies conducted in glacier-covered regions worldwide fail to take into account glacier water storage when estimating GWSA (Table S1).

On the other hand, although soil moisture storage is involved in most previous studies (Table S1), the adopted soil moisture data characterize water content within fixed-depth soil layers only instead of the entire soil profile. Among these data, soil moisture storage in the 0–200 cm soil layer simulated by GLDAS (Global Land Data Assimilation Systems) Noah (Rodell et al., 2004) has been most extensively applied. However, soil thickness is not spatially uniform in reality, and the 200 cm depth fails to represent actual soil profile depth in many regions. As early as 2001, Rodell and Famiglietti (2001) declared that a uniform soil depth of 200 cm would introduce significant uncertainties into GRACE-derived GWSA estimation. They defined the remaining water storage in the unsaturated zone below 200 cm as intermediate zone storage (IZS), a potentially critical but poorly understood component of TWS. When IZS is not quantified, it is unrealistic to clearly determine to what extent the separated GWSA variations are attributed to changes in actual groundwater level instead of changes in deep-layer soil moisture storage (Rodell and Famiglietti, 2002). In regions where soil moisture acts as the dominant component of TWS (Felfelani et al., 2017; Wang et al., 2018), the absence of deep-layer soil moisture storage will inevitably diminish the accuracy of GWSA estimation.

The primary objective of this study is to develop an improved GRACE-derived GWSA dataset at the global scale, namely igGWSA, by comprehensively considering diverse non-groundwater components and particularly resolving the effects of deep-layer soil moisture storage. igGWSA is expected to improve our understanding of the evolution of global and regional GWS, and to shed light on the scientific management and sustainable utilization of groundwater resources under a changing environment.

https://doi.org/10.5194/essd-2025-497
Preprint. Discussion started: 13 October 2025

2. Datasets

2.1. GRACE-based terrestrial water storage anomaly (TWSA) reconstruction data

In spite of the capability of providing global observations, the temporal gap existing between GRACE and GRACE-FO is not conducive to the analysis of TWS evolution. To this end, Li et al. (2021) reconstructed a long-term and gap-free TWSA dataset named GRID_CSR_GRACE_REC based on RL06 GRACE Mascon solutions. This reconstruction showed high consistency with RL06 GRACE-FO Mascon solutions and proved to be superior to previous TWSA datasets. Therefore, GRID_CSR_GRACE_REC was adopted in this study to encompass the entire period from 2000 to 2019.

2.2. Non-groundwater components data

2.2.1. Glaciers

Taking advantage of massive stereo images from the Advanced Spaceborne Thermal Estimation and Reflection Radiometer (ASTER), Hugonnet et al. (2021) developed a global-scale glacier mass balance dataset. Changes in glacier surface elevation, volume and mass were estimated at four levels of spatial resolution, i.e., $0.5^{\circ} \times 0.5^{\circ}$, $1^{\circ} \times 1^{\circ}$, $2^{\circ} \times 2^{\circ}$, and $4^{\circ} \times 4^{\circ}$. Volume change data with the finest resolution ($0.5^{\circ} \times 0.5^{\circ}$) were used in this study to obtain glacier water storage (Text S1).

2.2.2. Permafrost

Changes in permafrost water storage were indirectly estimated based on changes in active layer thickness (ALT) in this study (Text S2), as suggested by Xiang et al. (2016) and Zou et al. (2022). ALT data were derived from Community Land Model version 5 (CLM5) developed by the National Center for Atmospheric Research (NCAR).

2.2.3. Snow

Snow water equivalent simulations from seven reanalysis products were collected in this study, including: (1) GLDAS Noah from NASA (Rodell et al., 2004); (2) GLDAS Variable Infiltration

https://doi.org/10.5194/essd-2025-497
Preprint. Discussion started: 13 October 2025

Capacity (VIC) from NASA (Rodell et al., 2004); (3) GLDAS Catchment Land Surface Model (CLSM) from NASA (Rodell et al., 2004); (4) Famine Early Warning Systems Network Land Data Assimilation System (FLDAS) Noah from NASA (Mcnally et al., 2022); (5) Modern-Era Retrospective analysis for Research and Applications version 2 (MERRA-2) from NASA (Gelaro et al., 2017); (6) The land component dataset of the fifth generation of European ReAnalysis (ERA5-Land) from European Centre for Medium-Range Weather Forecasts (ECMWF) (Munoz-Sabater et al., 2021); (7) Japanese 55-year Reanalysis (JRA-55) from Japan Meteorological Agency (JMA) (Kobayashi et al., 2015).

2.2.4. Lakes and reservoirs

The global database of lake water storage (GLWS) developed by Yao et al. (2023) was used in this study. To construct GLWS, 248,649 satellite images from Landsat were used to map time-varying water areas (Yao et al., 2019). Then, elevation measurements from nine satellite altimeters, including CryoSat-2, ENVISAT, ICESat, ICESat-2, Jason 1-3, SARAL, and Sentinel 3, were used to estimate water levels. Lastly, changes in lake volume were quantified by combining water areas with water levels. GLWS depicts the variations in water storage of 1,972 large water bodies spanning 1992 to 2020, accounting for 96% of the total global lake water storage and 83% of the total global reservoir water storage, respectively. Data processing of GLWS is detailed in Text S3.

2.2.5. Surface runoff

The global runoff reanalysis reconstructed by Ghiggi et al. (2021), namely Global RUNoff ENSEMBLE (G-RUN ENSEMBLE), was used in this study. G-RUN ENSEMBLE is produced based on in situ river discharge measurements and machine learning. Benchmarked against other independent observations, this reanalysis outperforms simulations from a set of global hydrological models. A total of 21 atmospheric forcing datasets are involved to generate 525 ensemble members in G-RUN ENSEMBLE, and the median of all these members was adopted in our study.

2.2.6. Plant canopy water

Plant canopy water simulations from four reanalysis products were collected in this study, including: (1)

https://doi.org/10.5194/essd-2025-497
Preprint. Discussion started: 13 October 2025

GLDAS Noah; (2) GLDAS VIC; (3) GLDAS CLSM; (4) ERA5-Land.

2.2.7. Profile soil moisture (PSM)

In most GRACE-derived GWSA studies, the depth of soil moisture profile is set fixed, say 200 cm and 289 cm in Noah model driven by GLDAS and CHTESSEL model driven by ERA5, respectively. In this study, PSM simulated by CLSM was utilized. Inspired by Famiglietti and Wood (1994), Koster et al. (2000) and Ducharne et al. (2000) proposed CLSM in 2000 by coupling a classic hydrological model, TOPMODEL (Beven and Kirkby, 1979), with the parameterization of surface energy and water fluxes from Mosaic LSM. Based on the concepts of TOPMODEL, the distribution of water table depth can be inferred from that of topographic index. Subsequently, the distribution of water table depth is applied to derive catchment deficit (CD), which is defined as the water amount required to saturate the entire catchment under the assumption that vertical moisture profile in the unsaturated zone arises from hydrostatic equilibrium. In addition, two variables that take into account non-equilibrium conditions are defined in CLSM, namely surface excess (SE) and root zone excess (RE). SE and RE quantify the deviations of surface soil moisture and root zone soil moisture, respectively, from the value implied by the equilibrium profile. Richards equation is used to solve the vertical water fluxes between CD, SE, and RE, which contribute to bringing the vertical moisture profile closer to the equilibrium profile (Gascoin et al., 2009). Despite the significant value of CLSM-simulated PSM, uncertainties inherent to single-source simulation may inevitably compromise the accuracy of GWSA estimation. Thus, machine learning was applied in this study to improve CLSM-simulated PSM, as will be detailed in Sect. 3.2.

2.3. Predictor variables for PSM

Root zone soil moisture (RZSM), meteorological variables, and vegetation index were selected as predictor variables for PSM. As a function of vegetation type, root zone depth is characterized by spatial heterogeneity and is inherently challenging to quantify globally. In this study, soil water content within the uppermost 100 cm soil layer was defined as RZSM as suggested by Xu et al. (2021) and Heyvaert et al. (2023). RZSM simulations from five reanalysis products were collected, including: (1) GLDAS Noah; (2) GLDAS CLSM; (3) FLDAS Noah; (4) MERRA-2; (5) ERA5-Land. Data processing of RZSM is detailed in Text S4. With regard to meteorological variables, air temperature and precipitation from one of the most widely used climate dataset, CRU TS (Climatic Research Unit gridded Time Series) v4.08 (Harris et al., 2020), was adopted. Besides, the normalized difference vegetation index (NDVI) provided by Global Inventory Monitoring and Modeling System (GIMMS) (Pinzon and Tucker, 2014) was also used for prediction of PSM.

2.4. In situ-observed and model-simulated groundwater data

Jasechko et al. (2024) compiled in situ observations of groundwater level (GWL) from a total of 170,000 wells and 1,693 aquifer systems across more than 40 countries worldwide, with which they revealed widespread groundwater depletion in the 21st century. Due to the provisions of data sharing, only 59% of data used for analysis can be publicly accessed. The available data exhibit a pronounced spatial imbalance, with 97.7% of the monitoring wells located in the United States and the remaining 2.3% distributed across China, Canada, Europe, etc. In situ-observed GWL served as the benchmark for validating GWSA estimation in this study.

In addition, a state-of-the-art hydrological model coupled with human activity modules, namely the WaterGAP Global Hydrological Model (WGHM), was employed to provide independent simulations of GWSA. WaterGAP (Water-Global Assessment and Prognosis) is developed by the University of Frankfurt to quantify water storage, water resources, and water use at the global scale. GWSA simulations from the most recent version, i.e., WaterGAP v2.2e (Schmied et al., 2024), were used in this study.

Detailed information of data utilized in this study is listed in Table 1. Taking into account the spatiotemporal attributes of diverse datasets, this study was conducted over global land areas excluding Antarctica (60 °S–90 °N) at a $0.5^{\circ} \times 0.5^{\circ}$ spatial resolution, spanning the period from January 2000 to December 2019. Datasets with coarser resolutions were harmonized to $0.5^{\circ} \times 0.5^{\circ}$ by using bilinear interpolation.

https://doi.org/10.5194/essd-2025-497
Preprint. Discussion started: 13 October 2025

Table 1. Detailed descriptions of data utilized for generating igGWSA.

Variable	Data source	Time span	Temporal resolution	Spatial extent	Spatial resolution	Reference
TWS	GRID_CSR_GRACE_REC	1979–2020	monthly	60 °S–90 °N	0.5° × 0.5°	Li et al. (2021)
Glacier mass balance	ASTER-based	2000–2019	monthly	global	0.5° × 0.5°	Hugonnet et al. (2021)
Active layer thickness	CLM5	1850–present	monthly	global	1.25° × 0.9375°	Lawrence et al. (2019)
Snow water equivalent	GLDAS Noah	2000–present	monthly	60 °S–90 °N	0.25 ° × 0.25 °	Rodell et al. (2004)
	GLDAS VIC	2000–present	monthly	60 °S–90 °N	1 ° × 1 °	Rodell et al. (2004)
	GLDAS CLSM	2000–present	monthly	60 °S–90 °N	1 ° × 1 °	Rodell et al. (2004)
	FLDAS Noah	1982–present	monthly	60 °S–90 °N	0.1 ° × 0.1 °	Mcnally et al. (2022)
	MERRA-2	1980–present	monthly	60 °S–90 °N	0.625 ° × 0.5 °	Gelaro et al. (2017)
	ERA5-Land	1950–present	monthly	global	0.1 ° × 0.1 °	Muñoz-Sabater et al. (2021)
	JRA-55	1958–present	monthly	global	0.5625 ° × 0.5625 °	Kobayashi et al. (2015)
Lakes and reservoirs	GLWS	1992–2020	near-monthly	global	individual lake	Yao et al. (2023)
Surface runoff	G-RUN ENSEMBLE	1902–2019	monthly	global	0.5° × 0.5°	Ghiggi et al. (2021)
Plant canopy water	GLDAS Noah	2000–present	monthly	60 °S–90 °N	0.25 ° × 0.25 °	Rodell et al. (2004)
	GLDAS VIC	2000–present	monthly	60 °S–90 °N	1 ° × 1 °	Rodell et al. (2004)
	GLDAS CLSM	2000–present	monthly	60 °S–90 °N	1 ° × 1 °	Rodell et al. (2004)
	ERA5-Land	1950–present	monthly	global	0.1 ° × 0.1 °	Muñoz-Sabater et al. (2021)

https://doi.org/10.5194/essd-2025-497
Preprint. Discussion started: 13 October 2025

Table 1 (continued). Detailed descriptions of data utilized for generating igGWSA.

Variable	Data source	Time span	Temporal resolution	Spatial extent	Spatial resolution	Reference
Profile soil moisture	GLDAS CLSM	2000–present	monthly	60 °S–90 °N	1 °×1 °	Rodell et al. (2004)
Root zone soil moisture	GLDAS Noah	2000–present	monthly	60 °S–90 °N	0.25 °×0.25 °	Rodell et al. (2004)
	GLDAS CLSM	2000–present	monthly	60 °S–90 °N	1 °×1 °	Rodell et al. (2004)
	FLDAS Noah	1982–present	monthly	60 °S–90 °N	0.1 °×0.1 °	Mcnally et al. (2022)
	MERRA-2	1980–present	monthly	60 °S–90 °N	0.625 °×0.5 °	Gelaro et al. (2017)
	ERA5-Land	1950–present	monthly	global	0.1 °×0.1 °	Muñoz-Sabater et al. (2021)
Precipitation	CRU TS v4.08	1901–present	monthly	60 °S–90 °N	0.5° ×0.5°	Harris et al. (2020)
Temperature	CRU TS v4.08	1901–present	monthly	60 °S–90 °N	0.5° ×0.5°	Harris et al. (2020)
NDVI	GIMMS	1982–2022	semi-monthly	global	0.083° ×0.083°	Pinzon and Tucker (2014)
Groundwater level	in situ	well-dependent	yearly	global	individual well	Jasechko et al. (2024)
$GWSA_{WGHM}$	WaterGAP v2.2e	1901–2019	monthly	global	0.5° ×0.5°	Schmied et al. (2024)

https://doi.org/10.5194/essd-2025-497
Preprint. Discussion started: 13 October 2025

3. Methods

3.1. Integrating multi-source estimates via Bayesian three-cornered hat (BTCH)

BTCH proposed by He et al. (2020) is a data fusion method free of any a priori knowledge. By coupling TCH technique with Bayesian probabilistic frameworks, BTCH is capable of reducing uncertainties inherent to single-source dataset, and has been widely used to improve the estimation of hydrological variables such as soil moisture (Shangguan et al., 2023) and terrestrial water storage (Chen et al., 2024). In this study, BTCH was employed to generate ensemble simulations of snow water equivalent, plant canopy water and RZSM (Fig. 1, Text S5).

3.2. Generating PSM data with lower uncertainties via machine learning

3.2.1. Random forest (RF)

RF is an ensemble machine learning technique that combines decision tree with bagging algorithm (Breiman, 2001). In contrast to non-ensemble techniques, RF is characterized by stronger generalization ability, higher robustness to noise, and lower susceptibility to overfitting. Moreover, RF is more interpretable than other black-box machine learning methods owing to its capability to quantify the relative importance of predictors. RF has been extensively applied in soil moisture prediction (Wang et al., 2022; Li et al., 2022).

3.2.2. Modelling the relationship between PSM and covariates

RF was employed to establish relationship model between CLSM-simulated PSM and diverse covariates including CLSM-simulated RZSM, air temperature, precipitation, and NDVI (Fig. 1). There are two key hyperparameters in RF: the number of trees (*ntree*) and the number of variables randomly sampled as candidates at each split (*mtry*). We adjusted *ntree* from 250 to 1000 in steps of 250, and varied *mtry* from 1 to 4 (the total number of predictors) in steps of 1. All the remaining parameters were retained at their default settings. The 16 combinations of *ntree* and *mtry* were tested one by one, among which the one with the lowest prediction error was determined as the optimal parameter

https://doi.org/10.5194/essd-2025-497
Preprint. Discussion started: 13 October 2025

Earth System Science Data
Open Access Discussions

combination. Based on the optimal hyper-parameters, prediction models for PSM were developed at the pixel scale by randomly partitioning the datasets into training set and validation set at an 80%:20% ratio. The accuracy of RF model was evaluated using two metrics: R^2 (coefficient of determination) and rRMSE (relative root mean square error) (Text S6).

To further quantify the spatial differences in the accuracy of RF models, performance evaluation was also conducted at the climatic zone scale. Here, climate classification scheme based on aridity index (AI), the ratio of annual precipitation to potential evapotranspiration (PET), was adopted as suggested by the United Nations Environment Program (UNEP) (Middleton and Thomas, 1997). The climatology (1991–2020) of AI was computed using precipitation and PET data provided by CRU TS v4.08. Following the definition of UNEP, humid regions ($AI \geq 0.65$) and drylands ($AI<0.65$) were first delineated with a threshold of 0.65. Whereafter, drylands were further classified into four subtypes: dry sub-humid ($0.5 \leq AI < 0.65$), semi-arid ($0.2 \leq AI < 0.5$), arid ($0.05 \leq AI < 0.2$), and hyper-arid ($AI<0.05$).

3.2.3. Prediction of improved PSM and uncertainty analysis

Owing to the fact that PSM is inclusive of RZSM, this study assumed that RZSM served as a critical predictor for PSM. Accordingly, the prediction accuracy of PSM was expected to be enhanced by constraining the uncertainties in RZSM input. To this end, we integrated multi-source RZSM simulations by using BTCH. Given the established optimal models, ensemble RZSM, air temperature, precipitation, and NDVI were reintroduced as inputs into the models to derive improved prediction of PSM that synthesized the advantages of multi-source soil moisture datasets (Fig. 1).

Quantitative analysis was imperative to demonstrate whether the uncertainties in the improved prediction had been reduced relative to the original CLSM simulations. Typically, this can be achieved by using in situ measurements as benchmarks. Nevertheless, unlike surface soil moisture or RZSM, in situ-observed PSM is extremely scarce. In light of this, an alternative approach named the generalized three-corner hat (GTCH) (Tavella and Premoli, 1994) was used for uncertainty analysis. Note that at least three estimates are required to implement GTCH. Besides improved PSM and CLSM-simulated PSM, we additionally derived GLDAS-Noah-based PSM, FLDAS-Noah-based PSM,

https://doi.org/10.5194/essd-2025-497
Preprint. Discussion started: 13 October 2025

ERA5-Land-based PSM, and MERRA-2-based PSM by replacing the ensemble RZSM with the corresponding single-source RZSM as a model input. A dimensionless index, namely relative uncertainty, was calculated by GTCH to evaluate the abovementioned six PSM estimations from the perspective of uncertainties.

3.3. Estimation, validation and intercomparison methods of GWSA

3.3.1. Estimation of igGWSA and non-improved GWSA

Vertically, TWS comprises a variety of hydrological components such as glaciers, snow, soil moisture, groundwater, etc. By subtracting diverse non-groundwater components, GWS can be isolated from TWS (Fig. 1), as shown in Eq. (1).

$$igGWSA = TWSA - GlacierWSA - PWSA - LRWSA - SRSA - PSMSA_{improved} - SWEA - CWSA \ , \tag{1}$$

where $igGWSA$ stands for the improved estimation of groundwater storage anomaly; $TWSA$ is terrestrial water storage anomaly; $GlacierWSA$ is glacier water storage anomaly; $PWSA$ is permafrost water storage anomaly; $LRWSA$ is lake and reservoir water storage anomaly; $SRSA$ is surface runoff storage anomaly; $PSMSA_{improved}$ is the improved profile soil moisture storage anomaly; $SWEA$ is snow water equivalent anomaly; $CWSA$ is canopy water storage anomaly.

To quantify the impacts of incomprehensive considerations of non-groundwater components, five kinds of non-improved GWSA were further estimated as listed below.

(1) $GWSA_{simplified}$: Similar to most previous studies (Liu et al., 2023; Peng et al., 2021; Zhao et al., 2023), simplified GWSA was separated from TWSA by subtracting only soil moisture storage in the 0–200 cm soil layer, snow water equivalent, and plant canopy water simulated by GLDAS Noah.

(2) $GWSA_{CLSM}$: CLSM-simulated PSM instead of improved PSM was used to estimate GWSA, with all other non-groundwater components identical to those for igGWSA.

(3) $GWSA_{289}$: Soil moisture storage in the 0–289 cm soil layer derived from ERA5-Land instead of improved PSM was used to estimate GWSA, with all other non-groundwater components

https://doi.org/10.5194/essd-2025-497
Preprint. Discussion started: 13 October 2025

identical to those for igGWSA.

(4) $GWSA_{200}$: Soil moisture storage in the 0–200 cm soil layer derived from FLDAS Noah instead of improved PSM was used to estimate GWSA, with all other non-groundwater components identical to those for igGWSA.

(5) $GWSA_{ignored}$: GlacierWSA was ignored when estimating GWSA, with all other non-groundwater components identical to those for igGWSA.

3.3.2. Validation of igGWSA against in situ observations and model simulations

Focusing on the potential of igGWSA in detecting groundwater resources evolution and serving for global water security, validation of igGWSA was performed in five globally recognized hotspots of groundwater depletion, i.e., North China Plain, California Central Valley, High Plains of USA, Ganges-Brahmaputra River Basin, and the Middle East.

Among the five hotspots, high-density in situ observations of monitoring wells can be obtained from Jasechko et al. (2024) in North China Plain, California Central Valley, and High Plains of USA. Given the intrinsic disparity in spatial scales between in situ monitoring (point-scale) and igGWSA ($0.5^{o}\times 0.5^{o}$ grid cell), scale transformation was imperative before validation. Accordingly, point-scale data were first converted into pixel-scale by averaging observations of wells located in the specific grid cell. Then in situ GWL and GWSA estimation at a $0.5^{o}\times 0.5^{o}$ resolution were upscaled to obtain basin-averaged time series. Due to the fact that GWL and GWS are two fundamentally distinct hydrological variables, error metrics such as RSME were unsuitable for validation. Instead, Pearson's correlation coefficient (PCC) was employed to evaluate the consistency in their temporal evolution.

As for Ganges-Brahmaputra and the Middle East, in situ observations were currently unavailable. Alternatively, an advanced global hydrological model with consideration of effects of anthropogenic activities (e.g., water withdrawal) on groundwater resources, i.e., WGHM, was introduced to provide independent GWSA simulations. PCC between our igGWSA and WGHM-simulated GWSA was also calculated to facilitate the validation.

https://doi.org/10.5194/essd-2025-497
Preprint. Discussion started: 13 October 2025

3.3.3. Intercomparison between igGWSA and non-improved GWSA

Similar to intercomparison between various PSM estimations, GTCH was applied to quantify the relative uncertainty of igGWSA as well as four kinds of non-improved GWSA estimations, i.e., $GWSA_{simplified}$, $GWSA_{CLSM}$, $GWSA_{289}$, and $GWSA_{200}$. $GWSA_{ignored}$ was not involved in GTCH evaluation given that glaciers constitute only a minor fraction of global land areas.

In addition to pixel-wise uncertainty analysis, intercomparison between igGWSA and non-improved GWSA was further carried out under three kinds of distinctive geographical environments. To be specific, the three environments refer to glacier-covered regions, giant lakes, and deep-soil areas, corresponding to the absence of glaciers, lakes and reservoirs, and deep-layer soil moisture, respectively, in most previous studies when estimating GWSA in these regions.

For glacier-covered regions, a dataset of global glacier outlines named the Randolph Glacier Inventory (RGI) was utilized. RGI 6.0 defines 19 first-order glacier regions: (1) Alaska; (2) Western Canada and USA; (3) Arctic Canada (North); (4) Arctic Canada (South); (5) Greenland Periphery; (6) Iceland; (7) Svalbard and Jan Mayen; (8) Scandinavia; (9) Russian Arctic; (10) North Asia; (11) Central Europe; (12) Caucasus and Middle East; (13) Central Asia; (14) South Asia (West); (15) South Asia (East); (16) Low Latitudes; (17) Southern Andes; (18) New Zealand; (19) Antarctic and Subantarctic. Region 19 was excluded from analysis. Intercomparison between igGWSA and $GWSA_{ignored}$ was conducted in glacier-covered regions.

For giant lakes, 13 lakes or lake clusters were involved: (1) Caspian Sea; (2) Great Lakes of North America; (3) Victoria; (4) Tanganyika; (5) Baikal; (6) Great Bear; (7) Malawi; (8) Great Slave; (9) Winnipeg; (10) Ladoga; (11) Balkhash; (12) Aral Sea; (13) Lakes of Tibetan Plateau. The outlines of these lakes were derived from HydroLAKES dataset. Intercomparison between igGWSA and $GWSA_{simplified}$ was conducted in giant lakes.

For deep-soil areas, eight regions were selected as typical cases: (1) Mississippi River Basin; (2) Volga River Basin; (3) Ob River Basin; (4) Loess Plateau; (5) Congo River Basin; (6) Songhua-Liaohe River Basin; (7) Pampas Steppe; (8) Ganges-Brahmaputra River Basin. These regions were primarily determined based on soil depth information defined in GLDAS VIC model (Fig. S1) and encompassed the major loess and chernozem zones worldwide. Intercomparison between igGWSA, $GWSA_{289}$, and

https://doi.org/10.5194/essd-2025-497
Preprint. Discussion started: 13 October 2025

GWSA$_{200}$ was conducted in deep-soil areas.

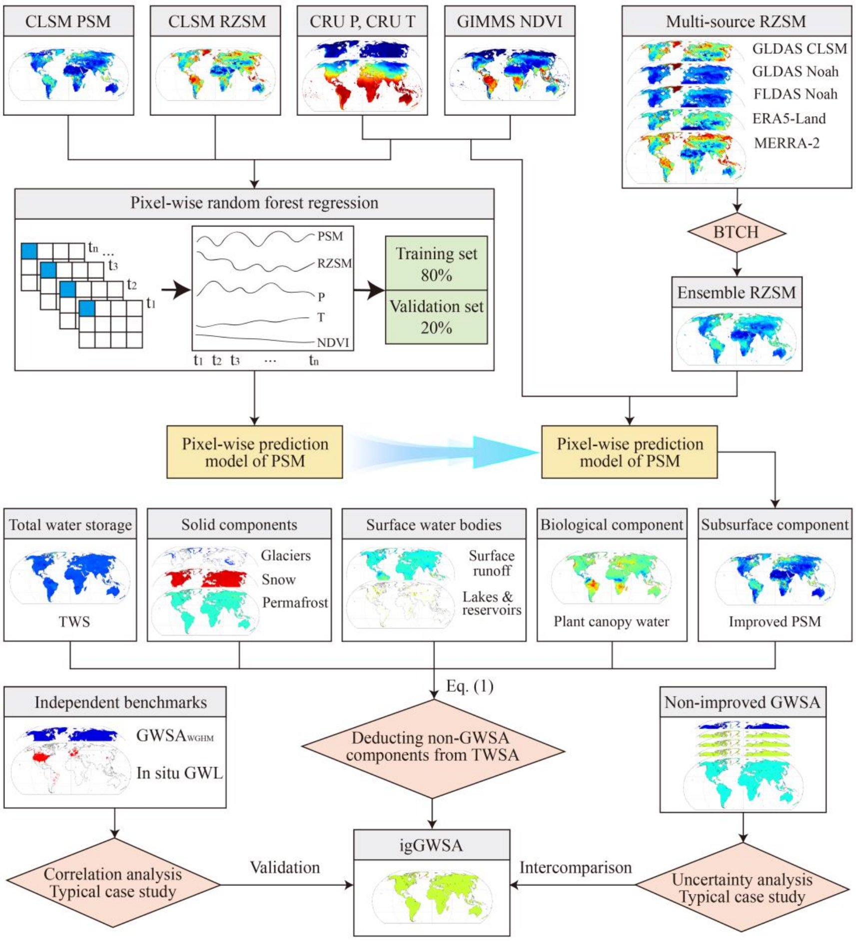

Figure 1. Flowchart of the generation process for igGWSA.

4. Results

4.1. Performance evaluation of RF-based modelling of PSM

4.1.1. Evaluation at the pixel scale

Pixel-wise RF models demonstrated exceptional accuracy in replicating CLSM-simulated PSM (Fig. 2). During model training, 86.90% and 97.33% of global grid cells achieved R^2 values exceeding 0.9 and 0.8, respectively, indicating strong explanatory power of the selected predictors for PSM. With regard

https://doi.org/10.5194/essd-2025-497
Preprint. Discussion started: 13 October 2025

to error metric, rRMSE was contained below 1% and 2% for 93.47% and 99.87% of global grid cells, respectively. The accuracy of validation sets was relatively lower than that of training sets, with 67.14% and 83.07% of grid cells exhibited R^2 values exceeding 0.9 and 0.8, respectively, and 76.96% and 97.43% of grid cells showed rRMSE less than 1% and 2%, respectively. Overall, the training and validation sets achieved average R^2 values of 0.96 and 0.89, respectively, with average rRMSE values of 1.18% and 1.84%.

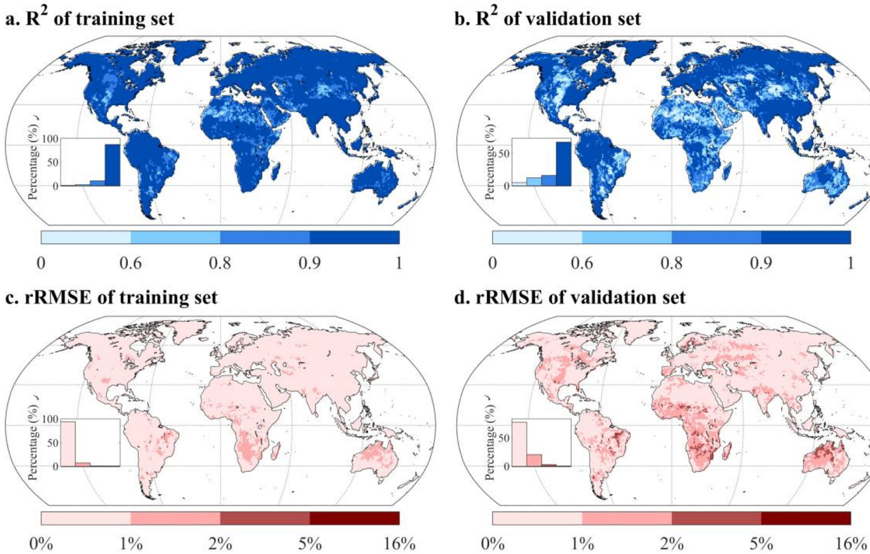

Figure 2. Pixel-scale performance of RF-based modelling of PSM.

4.1.2. Evaluation at the climatic zone scale

The accuracy of RF models was found to vary remarkably in different climatic zones. The models outperformed in humid regions compared to drylands, whether assessed through training/validation sets or evaluated by R^2/ rRMSE (Fig. 3). For the training set, the average R^2 values were 0.98 and 0.93 for humid regions and drylands, respectively, and the average rRMSE values were 1.10% and 1.29%, respectively. Moreover, the predictive skill of RF models was observed to progressively decline with increasing aridity within drylands: dry sub-humid (R^2=0.96), semi-arid (R^2=0.94), arid (R^2=0.92), and hyper-arid (R^2=0.87).

https://doi.org/10.5194/essd-2025-497
Preprint. Discussion started: 13 October 2025

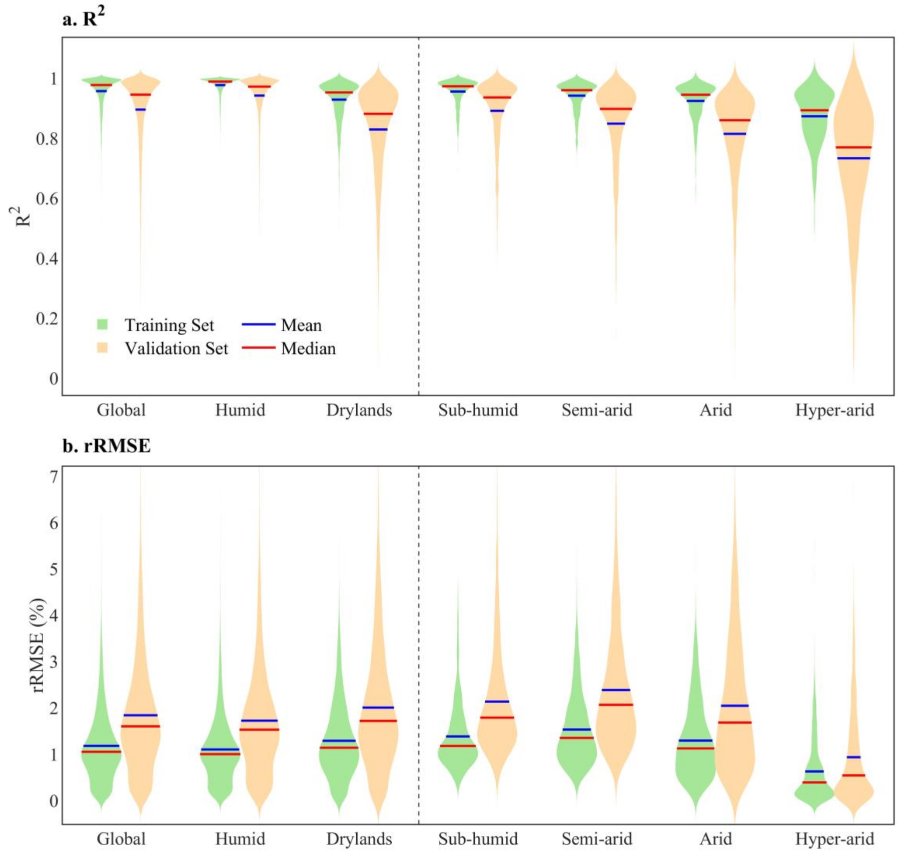

Figure 3. Climatic zone-scale performance of RF-based modelling of PSM.

4.1.3. Evaluation of interannual trends

The aforementioned evaluations were achieved by randomly partitioning time series of the given pixel into training and validation sets without maintaining the original patterns. Given this, evaluation of interannual trends in PSM was carried out additionally. Results showed that trends in RF-predicted PSM were highly consistent with trends in CLSM-simulated PSM with R^2 exceeding 0.98 in all climatic zones (Fig. 4). RF models effectively reproduced the interannual variations in PSM, which was critical for the temporal patterns of the derived GWSA.

https://doi.org/10.5194/essd-2025-497
Preprint. Discussion started: 13 October 2025

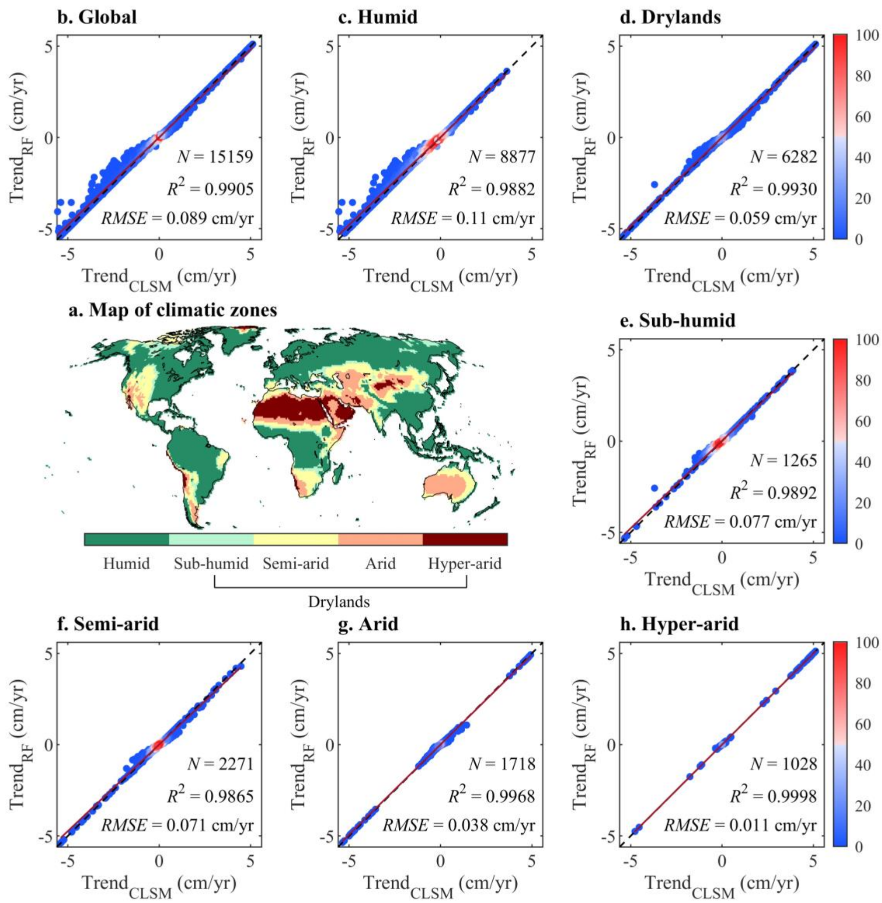

Figure 4. Comparison between trends in RF-predicted PSM and CLSM-simulated PSM.

4.2. Evaluation of improved estimation of PSM

4.2.1. Intercomparison with fixed-depth soil moisture

Improved estimation of PSM ($SMS_{profile}$) was compared to soil moisture storage in 0–200 cm layer (SMS_{200}) and 0–289 cm layer (SMS_{289}) (Fig. 5). The multi-year (2000–2019) and global averages of SMS_{200}, SMS_{289}, and $SMS_{profile}$ were 50.70 cm, 78.28 cm, and 106.98 cm, respectively. The spatial PCC between SMS_{200} and $SMS_{profile}$ was 0.55 (p<0.01), and that between SMS_{289} and $SMS_{profile}$ reached 0.74 (p<0.01). SMS_{289} was more comparable to $SMS_{profile}$ in both magnitude and spatial pattern, yet conspicuous deviations still existed. Therefore, fixed-depth soil moisture cannot adequately represent PSM, implying the considerable effects of deep-layer soil moisture.

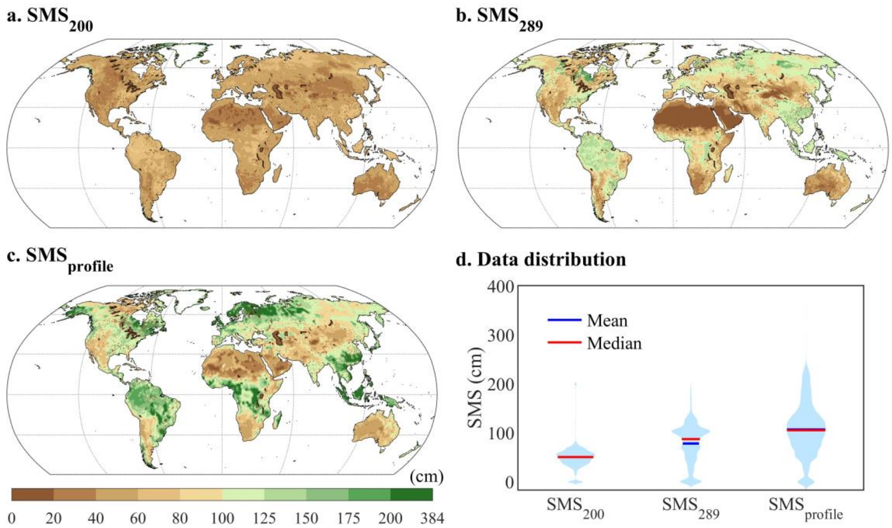

Figure 5. Intercomparison between SMS_{200}, SMS_{289}, and $SMS_{profile}$.

4.2.2. Intercomparison with single-source PSM estimations

Improved estimation of PSM was also compared to five kinds of single-source PSM estimations via GTCH (Fig. 6). The global-averaged relative uncertainty ranked as: CLSM-based PSM (0.057) > ERA5-Land-based PSM (0.048) > MERRA-2-based PSM (0.046) > GLDAS-Noah-based PSM (0.045) > FLDAS-Noah-based PSM (0.040) > ensemble-based PSM (0.019). CLSM-simulated PSM exhibited the highest uncertainty levels, whereas our improved PSM based on ensemble RZSM and RF modeling demonstrated the lowest relative uncertainty. Results confirmed that constraining the uncertainties of predictors can effectively improve the accuracy of PSM estimation.

https://doi.org/10.5194/essd-2025-497
Preprint. Discussion started: 13 October 2025

Open Access Earth System Science Data Discussions

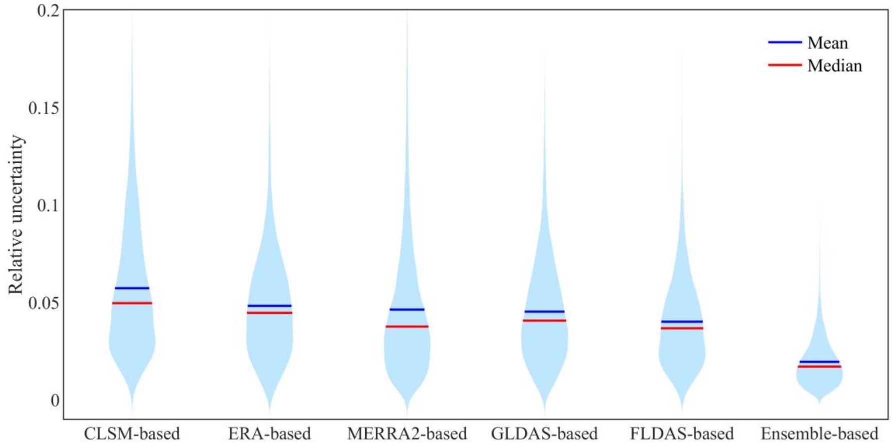

Figure 6. Relative uncertainty of ensemble-based PSM and single-source PSM.

4.3. Evaluation of igGWSA

4.3.1. Validation against in situ observations and model simulations

Well-monitored groundwater depth ($GWD_{in\ situ}$, negatively correlated with GWL) and WGHM-simulated GWSA ($GWSA_{WGHM}$) were applied as independent benchmarks to validate igGWSA in five typical hotspots (Fig. 7). PCCs between igGWSA and $GWD_{in\ situ}$ reached −0.99 (p<0.01), −0.95 (p<0.01), and −0.96 (p<0.01) in North China Plain, Central Valley, and High Plains, respectively. Persistent declines in GWS were accompanied by distinct increases in GWD, both indicating substantial mass loss. For all the five hotspots, tremendous groundwater depletion revealed by igGWSA was highly consistent with $GWSA_{WGHM}$ in spite of differences in declining rates, with PCCs ranging from 0.95 (p<0.01) to 0.99 (p<0.01). Validation results suggested that igGWSA was capable of detecting temporal evolution of groundwater resources. Unlike our comprehensive method, Jin and Feng (2013) obtained two GRACE-derived GWSA estimations based on GLDAS and WGHM by using simplified method and found that the amplitudes of $GWSA_{WGHM}$ were much smaller than these two simplified estimations. In comparison, our igGWSA are in high agreement with $GWSA_{WGHM}$ as demonstrated above, underscoring the importance of the full consideration of non-groundwater storage components.

https://doi.org/10.5194/essd-2025-497
Preprint. Discussion started: 13 October 2025

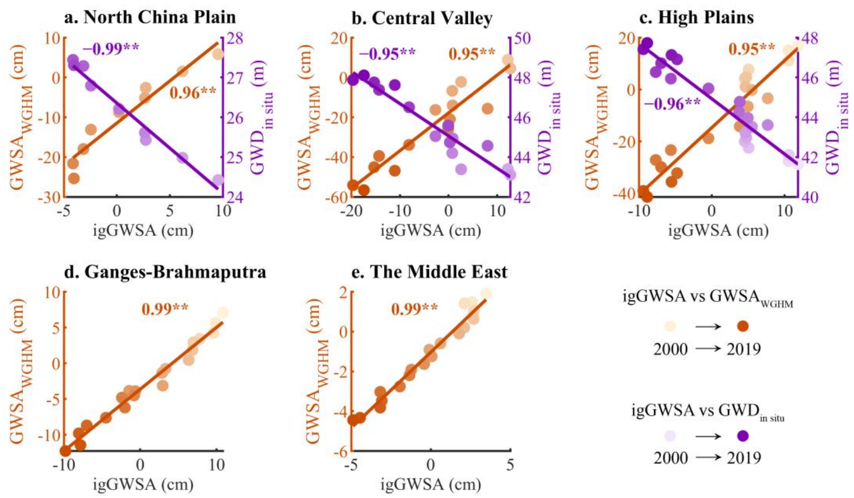

Figure 7. Validation of igGWSA against $GWD_{in\ situ}$ and $GWSA_{WGHM}$ in five typical hotspots of groundwater depletion. ** indicates significance at the 0.01 level.

4.3.2. Uncertainty analysis

Uncertainty analysis was further conducted for igGWSA and four kinds of non-improved estimations (Fig. 8). The global-averaged relative uncertainty ranked as: $GWSA_{simplified}$ (0.94) > $GWSA_{289}$ (0.74) > $GWSA_{CLSM}$ (0.67) > $GWSA_{200}$ (0.59) > igGWSA (0.56). The highest uncertainty was observed in $GWSA_{simplified}$, which was estimated by roughly deducting only fixed-depth soil moisture, snow, and plant canopy water from TWS like most previous studies. In contrast, our igGWSA that comprehensively took into account diverse non-groundwater components exhibited the lowest uncertainty. Note that $GWSA_{CLSM}$ relying on CLSM-simulated PSM showed higher uncertainty than igGWSA, highlighting the significance of improving GWSA estimation by optimizing PSM simulation.

https://doi.org/10.5194/essd-2025-497
Preprint. Discussion started: 13 October 2025

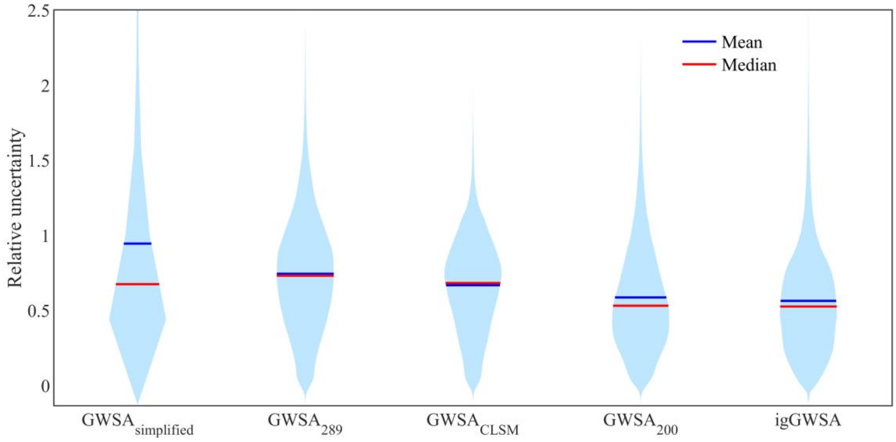

Figure 8. Relative uncertainty of igGWSA and non-improved estimations of GWSA.

4.4. Intercomparison between igGWSA and non-improved GWSA under distinctive geographical environments

4.4.1. Glacier-covered regions

The impacts of neglecting glacier water storage on the estimation of GWSA in glacier-covered regions manifested as three scenarios (Fig. 9, Table S2):

(1) Misestimation of the sign of trends: In Region 1, 3, 4, 6, 7, 11, 13, 14, 15, and 17, GWS tended to increase significantly due to the replenishment from glacier meltwater. However, the potential increasing trends would be reversed when ignoring glacier as a non-groundwater component.

(2) Overestimation of the decreasing trends: Both igGWSA and $GWSA_{ignored}$ were observed to decrease, but the latter exhibited a more considerable declining rate on account of the additional contribution of changes in glacier. This pattern was found in Region 5, 9, and 12.

(3) Underestimation of the increasing trends: Compared to igGWSA that increased at a remarkable rate, the increasing trend of $GWSA_{ignored}$ was greatly offset by glacier melting. This pattern was represented by Region 2, 8, 10, 16, and 18.

Regarding to the global glaciated areas, igGWSA and $GWSA_{ignored}$ declined at rates of −0.19 cm/yr (p<0.01) and −4.03 cm/yr (p<0.01), respectively. However, the enormous mass loss signal was primarily attributed to glacier melting (−3.85 cm/yr, p<0.01) rather than groundwater depletion itself.

https://doi.org/10.5194/essd-2025-497
Preprint. Discussion started: 13 October 2025

Therefore, absence of glaciers would inevitably result in inaccurate estimation of GWSA and misunderstandings of GWS evolution in glacier-covered regions.

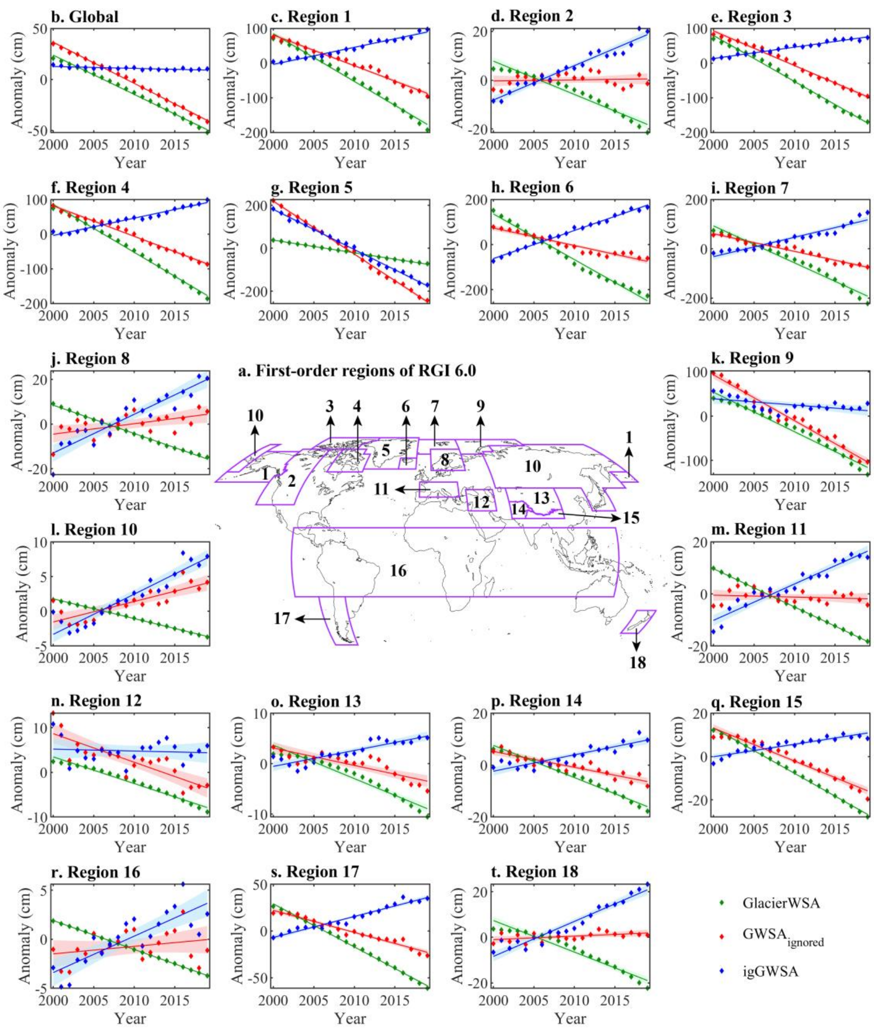

Figure 9. Intercomparison between igGWSA and GWSA$_{ignored}$ in glacier-covered regions.

4.4.2. Giant lakes

Among the 13 giant lakes, Tanganyika, Great Bear, Great Slave, Winnipeg, and Ladoga exhibited insignificant ($p \geq 0.05$) fluctuations in water storage. For the remaining eight lakes where dramatic storage variations have been detected, GWSA$_{simplified}$ can lead to two kinds of diametrically opposed

https://doi.org/10.5194/essd-2025-497
Preprint. Discussion started: 13 October 2025

misinterpretations (Fig. 10, Table S3).

(1) For shrinking lakes including Caspian Sea, Baikal, Malawi, and Aral Sea, increasing signals of GWS were overshadowed by the pronounced declining signals of lake water storage, thus indicating unrealistic risks of groundwater depletion.

(2) For expanded lakes including Great Lakes of NA, Victoria, Balkhash, and Lakes of Tibetan Plateau, decreasing trends in GWS became unrecognizable due to the marked increasing trends in lake water storage, consequently generating spurious positive signals of groundwater surplus. This is what was exactly presented in Jin and Feng (2013).

For all the 1,972 large lakes and reservoirs worldwide, igGWSA and $GWSA_{simplified}$ showed a decreasing trend of −0.19 cm/yr (p<0.01) and −0.35 cm/yr (p<0.01), respectively. $GWSA_{simplified}$ interpreted mass loss of surface water bodies (−0.11 cm/yr, p>0.05) as part of changes in GWS, which significantly exaggerated groundwater depletion at the global scale.

https://doi.org/10.5194/essd-2025-497
Preprint. Discussion started: 13 October 2025

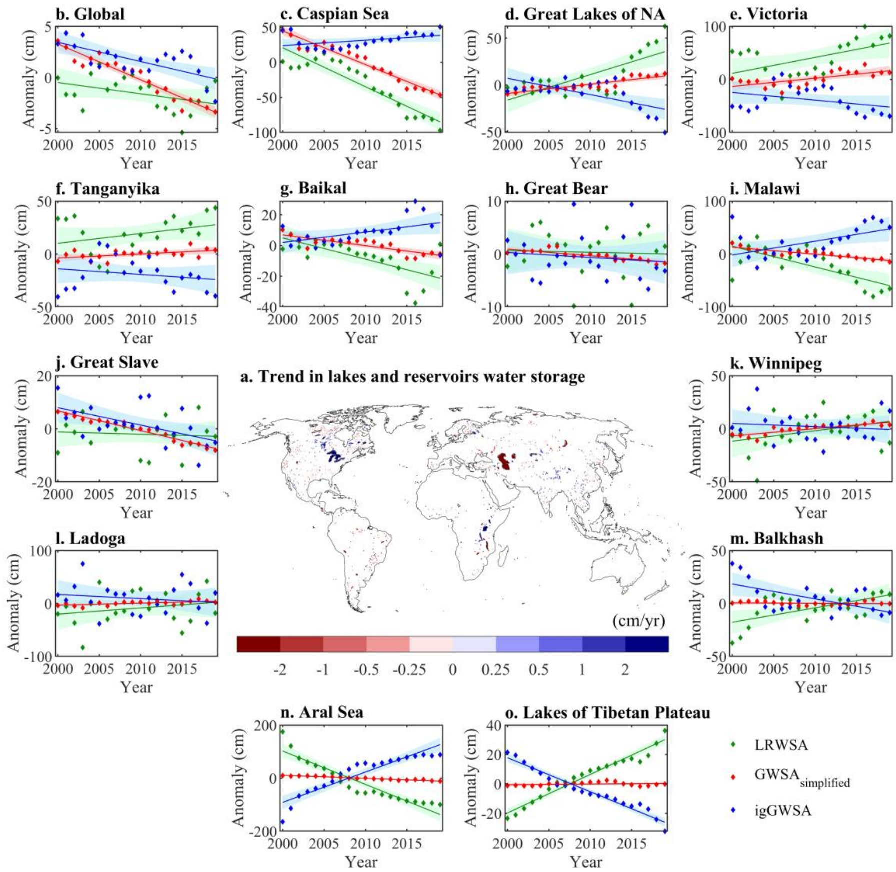

Figure 10. Intercomparison between igGWSA and GWSA$_{simplified}$ in giant lakes.

4.4.3. Deep-soil areas

Non-improved GWSA based on fixed-depth SM (GWSA$_{200}$, GWSA$_{289}$) demonstrated consistent sign of interannual trends with igGWSA in only four of the eight deep-soil regions, i.e., Mississippi, Volga, Loess Plateau, and Ganges-Brahmaputra (Fig. 11, Table S4). GWSA$_{200}$ showed an opposite trend to igGWSA in Ob and Congo, and negative correlation was found between GWSA$_{289}$ and igGWSA in Songhua-Liaohe and Pampas. Beyond the sign, the magnitude of trends in GWSA$_{200}$, GWSA$_{289}$, and igGWSA also varied considerably. For instance, igGWSA exhibited insignificant fluctuations with absolute rates not exceeding 0.1 cm/yr in Ob, Congo, Songhua-Liaohe and Pampas. However, GWSA$_{289}$ increased significantly with rates ranging from 0.22 cm/yr to 0.69 cm/yr in these regions. Results underscored the limitations of fixed-depth SM data and the necessity of involving deep-layer

https://doi.org/10.5194/essd-2025-497
Preprint. Discussion started: 13 October 2025

soil moisture as a non-groundwater component.

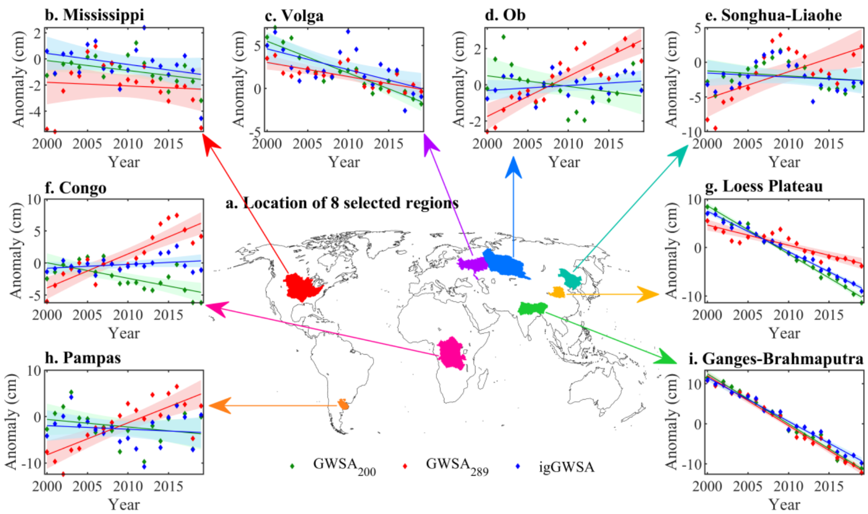

Figure 11. Intercomparison between $GWSA_{200}$, $GWSA_{289}$, and igGWSA in deep-soil areas.

5. Discussions

5.1. Influence factors of PSM modelling

In the RF-based modelling of CLSM-simulated PSM, CLSM-simulated RZSM achieved the highest importance among the four predictors across 97.17% of global grid cells (Fig. 12), implying the feasibility of improving PSM simulations by optimizing RZSM. Despite this, CLSM-simulated RZSM outperformed other RZSM products only in 16.10% of global grid cells (Fig. S2). The optimal RZSM product was characterized by strong spatial heterogeneity without any dominant patterns, which underscored the significance of integrating multi-source RZSM simulations for PSM prediction. Furthermore, the relative importance of RZSM varied with climate conditions. Specifically, it was more important in humid regions than in drylands as illustrated by scaled importance (Fig. S3). This implied the weaker correlation between RZSM and PSM in drylands, which explained the lower R^2 of RF models in drylands mentioned in Sect. 4.1.2, given that RZSM was the foremost predictor of PSM. We attributed the differences across climatic zones to the higher susceptibility to decoupling of RZSM and PSM in drylands, which was consistent to Carranza et al. (2018) who identified decoupling of

https://doi.org/10.5194/essd-2025-497
Preprint. Discussion started: 13 October 2025

surface and subsurface SM under arid conditions with in situ data.

For the remaining 2.83% of global grid cells, NDVI emerged as the dominant predictor variable for PSM modelling in most regions, accounting for 2.08% of global grid cells in total. Specifically, NDVI exhibited predominant impacts on PSM dynamics in the band between the Sahara Desert and the Congo Basin, the east coast of Africa, eastern South America, and northern Australia (Fig. 12). Interestingly, this spatial pattern closely aligned with the global distribution of deep-rooted regions predicted by Schenk and Jackson (2005) via climate-based model, highlighting the critical role of vegetation activity in regulating regional water storage variability. To further investigate the relationship between vegetation and water storage, the spatiotemporal variations of the sole vegetation-associated TWS component, i.e., canopy water storage (CWS), were analyzed (Fig. S4). However, the spatial pattern of CWS failed to match that of the variable importance of NDVI. The reason may be that CWS cannot adequately represent vegetation water storage, which was not quantified in this study due to its markedly smaller magnitude of variation compared to other components at the global scale (Rodell et al., 2005). Building on these findings, we suggest that vegetation water storage should be underscored in the hotspots of vegetation-PSM interactions to enhance the understanding of regional water storage evolution in future studies.

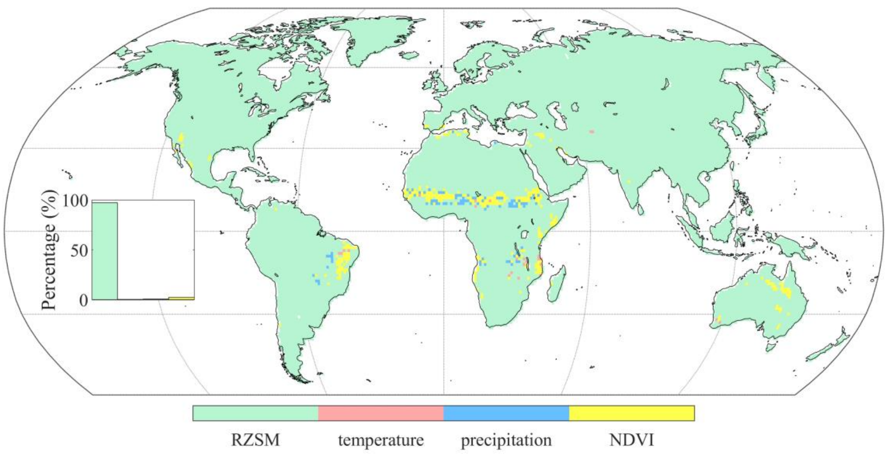

Figure 12. Map of dominant predictor variable for PSM modelling.

https://doi.org/10.5194/essd-2025-497
Preprint. Discussion started: 13 October 2025

Open Access Earth System Science Data Discussions

5.2. The gains to GWSA estimation from improved PSM

As demonstrated in Sect. 4.3.2, igGWSA based on improved PSM achieved lower uncertainty compared to $GWSA_{CLSM}$ based on CLSM-simulated PSM. To substantiate the gains from improved PSM to GWSA estimation, igGWSA and $GWSA_{CLSM}$ were further compared using $GWD_{in\ situ}$ as benchmarks.

At the pixel scale, igGWSA showed average PCCs of −0.41, −0.71, −0.70, and −0.58 with $GWD_{in\ situ}$ in North China Plain (NCP) , Central Valley (CV) , High Plains (HP) , and the aggregation of these three hotspots, respectively. In contrast, average PCCs between $GWSA_{CLSM}$ and $GWD_{in\ situ}$ were −0.38, −0.73, −0.59, and −0.51 in these regions (Table 2). igGWSA achieved stronger correlations with $GWD_{in\ situ}$ except in CV where only seven pixels were involved in analysis. Mann-Whitney U test was adopted to further identify the differences between igGWSA and $GWSA_{CLSM}$. The differences were not statistically significant in NCP and CV, while igGWSA was significantly superior to $GWSA_{CLSM}$ in HP and the aggregation (Fig. 13).

At the regional scale, igGWSA and $GWSA_{CLSM}$ exhibited comparable correlations with $GWD_{in\ situ}$ in NCP and CV, with difference in PCCs not exceeding 0.02. As for HP, igGWSA was relatively more notably correlated with $GWD_{in\ situ}$ than $GWSA_{CLSM}$ (−0.96 vs −0.90) (Table 2). In conclusion, improving PSM via machining learning was of great significance for generating GWSA estimation with higher accuracy and lower uncertainty.

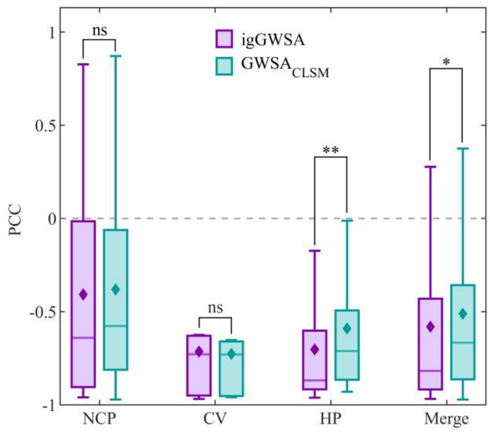

Figure 13. Difference in PCC between igGWSA and $GWD_{in\ situ}$ versus $GWSA_{CLSM}$ and $GWD_{in\ situ}$. **

https://doi.org/10.5194/essd-2025-497
Preprint. Discussion started: 13 October 2025

indicates significance at the 0.01 level; * indicates significance at the 0.05 level; ns indicates not significant (*p* > 0.05).

Table 2. Correlations of igGWSA and $GWSA_{CLSM}$ with $GWD_{in\ situ}$ at the pixel scale and the regional scale.

Region	Pixel_N	Pixel scale		Regional scale	
		igGWSA	$GWSA_{CLSM}$	igGWSA	$GWSA_{CLSM}$
NCP	48	−0.41	−0.38	−0.99**	−0.98**
CV	7	−0.71	−0.73	−0.95**	−0.97**
HP	61	−0.70	−0.59	−0.96**	−0.90**
Merge	116	−0.58	−0.51	/	/

Note: Pixel_N indicates the number of pixels at a $0.5^{\circ}\times0.5^{\circ}$ resolution in the specific region; ** indicates significance at the 0.01 level; Values for pixel scale indicates the average of PCCs for all pixels.

5.3. Uncertainties and limitations

Although GRACE provides an innovative perspective for monitoring GWS, it is essentially an indirect estimation methodology. Uncertainties inherent in TWSA data and non-groundwater components data will ultimately propagate into GRACE-derived GWSA. Therefore, validation of igGWSA against in situ measurements is imperative. However, existing as a conceptual derivative of TWSA, GWSA lacks ground truth. Given that, GWL data collected from monitoring wells can serve as substitute benchmarks for validating GWSA. It should be noted that GWL is closely linked to but is not directly comparable to GWSA. Accordingly, only correlation metric was employed for validation without error quantification in this study. Moreover, as mentioned in Sect. 1, the scarcity of globally accessible groundwater monitoring data renders large-scale validation of GWSA infeasible. To address this, local-scale validation was alternatively conducted focusing on several hotspots of groundwater depletion in this study based on available in situ observations and model simulations accounting for human water use. We would greatly appreciate if researchers worldwide could carry out supplementary validation of igGWSA using locally available in situ data.

https://doi.org/10.5194/essd-2025-497
Preprint. Discussion started: 13 October 2025

6. Data availability

Datasets used to develop igGWSA are publicly available and have been stated in the Datasets section. Our igGWSA dataset is archived on Zenodo and can be freely downloaded at https://doi.org/10.5281/zenodo.16871689 (Wang et al., 2025).

7. Conclusions

An improved GRACE-derived GWSA dataset over global land, namely igGWSA, was developed in this study. To this end, we first generated improved estimation of PSM based on RF algorithm and multi-source RZSM simulations. Then diverse non-groundwater components were subtracted from TWSA to obtain igGWSA. Finally, validation of igGWSA against in situ observations and model simulations and intercomparison between igGWSA and non-improved GWSA were conducted. The key conclusions can be summarized as follows:

(1) RF-based modeling of PSM exhibited superior performance at the global scale, with average R^2 and rRMSE reaching 0.96 and 1.18%, respectively. RF models outperformed in humid regions over drylands Among the predictors, RZSM showed the highest explanatory power for PSM variations, implying the feasibility of improving PSM by optimizing RZSM. The improved PSM estimation integrating multi-source RZSM exhibited the lowest relative uncertainty compared to estimations based on single-source RZSM.

(2) igGWSA was highly consistent with in situ-observed GWD and WGHM-simulated GWSA in five typical hotspots of groundwater depletion worldwide, i.e., North China Plain, California Central Valley, High Plains of USA, Ganges-Brahmaputra, and the Middle East, with |PCC| ranging from 0.89 to 0.99. In addition, igGWSA exhibited the lowest relative uncertainty compared to four kinds of non-improved GWSA estimations, including $GWSA_{CLSM}$ that relied on CLSM-simulated PSM. Furthermore, igGWSA also achieved significantly stronger correlations with in situ observations than $GWSA_{CLSM}$, underscoring the gains from improved PSM to GWSA estimation.

(3) igGWSA and non-improved GWSA estimations showed remarkable discrepancies in

https://doi.org/10.5194/essd-2025-497
Preprint. Discussion started: 13 October 2025

glacier-covered regions, giant lakes, and deep-soil areas. Specifically, neglecting glacier as a non-groundwater component would erroneously attribute mass loss induced by glacier melting to groundwater depletion. Similarly, simplified estimation without considering lakes and reservoirs would confound the signals of lake shrinkage or expansion with changes in GWS. Besides, GWSA estimations based on fixed-depth SM would fail to satisfactorily replicate the sign and the magnitude of trends in igGWSA due to the absence of deep-layer soil moisture storage.

Author contributions. ZW: Data curation, methodology, software, conceptualization, writing–original draft, writing – review & editing. SL: Conceptualization, supervision, writing – review & editing, project administration, funding acquisition. XM: Supervision, writing – review & editing, project administration, funding acquisition.

Competing interests. The contact author has declared that none of the authors has any competing interests.

Acknowledgements. The authors would like to thank the institutions and scientists who contributed invaluable data to the generation of our igGWSA dataset.

Financial support. This work was supported by National Key Research and Development Program of China (Grant No. 2022YFF0801804), China National Natural Science Foundation Projects (Grant Nos. 12441511 and 12441501) and the Third Xinjiang Scientific Expedition Program (Grant No. 2021xjkk0803).

References

Adams, K. H., Reager, J. T., Rosen, P., Wiese, D. N., Farr, T. G., Rao, S., Haines, B. J., Argus, D. F., Liu, Z., Smith, R., Famiglietti, J. S., and Rodell, M.: Remote sensing of groundwater: current capabilities and future directions, Water Resour. Res., 58, e2022WR032219, https://doi.org/10.1029/2022wr032219, 2022.

Berghuijs, W. R., Luijendijk, E., Moeck, C., van der Velde, Y., and Allen, S. T.: Global recharge data set

https://doi.org/10.5194/essd-2025-497
Preprint. Discussion started: 13 October 2025

indicates strengthened groundwater connection to surface fluxes, Geophys. Res. Lett., 49, e2022GL099010, https://doi.org/10.1029/2022gl099010, 2022.

Beven, K. J. and Kirkby, M. J.: A physically based variable contributive area model of basin hydrology, Hydrol. Sci. Bull., 24, 43–69, https://doi.org/10.1080/02626667909491834, 1979.

Breiman, L.: Random forests, Mach. Learn., 45, 5-32, https://doi.org/10.1023/a:1010933404324, 2001.

Carranza, C. D. U., van der Ploeg, M. J., and Torfs, P. J. J. F.: Using lagged dependence to identify (de) coupled surface and subsurface soil moisture values, Hydrol. Earth Syst. Sci., 22, 2255-2267, https://doi.org/10.5194/hess-22-2255-2018, 2018.

Chen, W., Forootan, E., Shum, C. K., Zhong, M., Feng, W., Xiong, Y., and Li, W.: A novel dynamic scale factor designed for recovering global TWS changes, J. Hydrol., 637, 131364, https://doi.org/10.1016/j.jhydrol.2024.131364, 2024.

Condon, L. E., Atchley, A. L., and Maxwell, R. M.: Evapotranspiration depletes groundwater under warming over the contiguous United States, Nat. Commun., 11, 873, https://doi.org/10.1038/s41467-020-14688-0, 2020.

de Graaf, I. E. M., Marinelli, B., and Liu, S.: Global analysis of groundwater pumping from increased river capture, Environ. Res. Lett., 19, 044064, https://doi.org/10.1088/1748-9326/ad383d, 2024.

de Graaf, I. E. M., van Beek, R. L. P. H., Gleeson, T., Moosdorf, N., Schmitz, O., Sutanudjaja, E. H., and Bierkens, M. F. P.: A global-scale two-layer transient groundwater model: development and application to groundwater depletion, Adv. Water Resour., 102, 53-67, https://doi.org/10.1016/j.advwatres.2017.01.011, 2017.

Döll, P. and Fiedler, K.: Global-scale modeling of groundwater recharge, Hydrol. Earth Syst. Sci., 12, 863-885, https://doi.org/10.5194/hess-12-863-2008, 2008.

Ducharne, A., Koster, R. D., Suarez, M. J., Stieglitz, M., and Kumar, P.: A catchment-based approach to modeling land surface processes in a general circulation model 2. Parameter estimation and model demonstration, J. Geophys. Res.: Atmos., 105, 24823-24838, https://doi.org/10.1029/2000jd900328, 2000.

Famiglietti, J. S. and Wood, E. F.: Multiscale modeling of spatially-variable water and energy-balance processes, Water Resour. Res., 30, 3061-3078, https://doi.org/10.1029/94wr01498, 1994.

Fan, Y., Li, H., and Miguez-Macho, G.: Global patterns of groundwater table depth, Science, 339, 940-943, https://doi.org/10.1126/science.1229881, 2013.

Felfelani, F., Wada, Y., Longuevergne, L., and Pokhrel, Y. N.: Natural and human-induced terrestrial water storage change: a global analysis using hydrological models and GRACE, J. Hydrol., 553, 105-118, https://doi.org/10.1016/j.jhydrol.2017.07.048, 2017.

Gascoin, S., Ducharne, A., Ribstein, P., Carli, M., and Habets, F.: Adaptation of a catchment-based land surface model to the hydrogeological setting of the Somme River basin (France), J. Hydrol., 368, 105-116, https://doi.org/10.1016/j.jhydrol.2009.01.039, 2009.

Gelaro, R., McCarty, W., Suarez, M. J., Todling, R., Molod, A., Takacs, L., Randles, C. A., Darmenov, A., Bosilovich, M. G., Reichle, R., Wargan, K., Coy, L., Cullather, R., Draper, C., Akella, S., Buchard, V., Conaty, A., da Silva, A. M., Gu, W., Kim, G.-K., Koster, R., Lucchesi, R., Merkova, D., Nielsen, J. E., Partyka, G., Pawson, S., Putman, W., Rienecker, M., Schubert, S. D., Sienkiewicz, M., and Zhao, B.: The Modern-Era Retrospective Analysis for Research and Applications, version 2 (MERRA-2), J. Clim., 30, 5419-5454, https://doi.org/10.1175/jcli-d-16-0758.1, 2017.

https://doi.org/10.5194/essd-2025-497
Preprint. Discussion started: 13 October 2025

Ghiggi, G., Humphrey, V., Seneviratne, S. I., and Gudmundsson, L.: G-RUN ENSEMBLE: A multi-forcing observation-based global runoff reanalysis, Water Resour. Res., 57, e2020WR028787, https://doi.org/10.1029/2020wr028787, 2021.

Gleeson, T., Cuthbert, M., Ferguson, G., and Perrone, D.: Global groundwater sustainability, resources, and systems in the Anthropocene, Annu. Rev. Earth Planet. Sci., 48, 431-463, https://doi.org/10.1146/annurev-earth-071719-055251, 2020.

Gleeson, T., Wada, Y., Bierkens, M. F. P., and van Beek, L. P. H.: Water balance of global aquifers revealed by groundwater footprint, Nature, 488, 197-200, https://doi.org/10.1038/nature11295, 2012.

Harris, I., Osborn, T. J., Jones, P., and Lister, D.: Version 4 of the CRU TS monthly high-resolution gridded multivariate climate dataset, Sci. Data, 7, 109, https://doi.org/10.1038/s41597-020-0453-3, 2020.

Hasan, M. F., Smith, R., Vajedian, S., Pommerenke, R., and Majumdar, S.: Global land subsidence mapping reveals widespread loss of aquifer storage capacity, Nat. Commun., 14, 6180, https://doi.org/10.1038/s41467-023-41933-z, 2023.

He, X., Xu, T., Xia, Y., Bateni, S. M., Guo, Z., Liu, S., Mao, K., Zhang, Y., Feng, H., and Zhao, J.: A Bayesian three-cornered hat (BTCH) method: improving the terrestrial evapotranspiration estimation, Remote Sens., 12, 878, https://doi.org/10.3390/rs12050878, 2020.

Heyvaert, Z., Scherrer, S., Bechtold, M., Gruber, A., Dorigo, W., Kumar, S., and De Lannoy, G.: Impact of design factors for ESA CCI satellite soil moisture data assimilation over Europe, J. Hydrometeorol., 24, 1193-1208, https://doi.org/10.1175/jhm-d-22-0141.1, 2023.

Hugonnet, R., McNabb, R., Berthier, E., Menounos, B., Nuth, C., Girod, L., Farinotti, D., Huss, M., Dussaillant, I., Brun, F., and Kaab, A.: Accelerated global glacier mass loss in the early twenty-first century, Nature, 592, 726-731, https://doi.org/10.1038/s41586-021-03436-z, 2021.

Jasechko, S., Seybold, H., Perrone, D., Fan, Y., Shamsudduha, M., Taylor, R. G., Fallatah, O., and Kirchner, J. W.: Rapid groundwater decline and some cases of recovery in aquifers globally, Nature, 625, 715-721, https://doi.org/10.1038/s41586-023-06879-8, 2024.

Jin, S. and Feng, G.: Large-scale variations of global groundwater from satellite gravimetry and hydrological models, 2002-2012, Global Planet. Change, 106, 20-30, https://doi.org/10.1016/j.gloplacha.2013.02.008, 2013.

Kobayashi, S., Ota, Y., Harada, Y., Ebita, A., Moriya, M., Onoda, H., Onogi, K., Kamahori, H., Kobayashi, C., Endo, H., Miyaoka, K., and Takahashi, K.: The JRA-55 reanalysis: general specifications and basic characteristics, J. Meteorolog. Soc. Jpn., 93, 5-48, https://doi.org/10.2151/jmsj.2015-001, 2015.

Koster, R. D., Suarez, M. J., Ducharne, A., Stieglitz, M., and Kumar, P.: A catchment-based approach to modeling land surface processes in a general circulation model 1. Model structure, J. Geophys. Res.: Atmos., 105, 24809-24822, https://doi.org/10.1029/2000jd900327, 2000.

Kuang, X., Liu, J., Scanlon, B. R., Jiao, J. J., Jasechko, S., Lancia, M., Biskaborn, B. K., Wada, Y., Li, H., Zeng, Z., Guo, Z., Yao, Y., Gleeson, T., Nicot, J.-P., Luo, X., Zou, Y., and Zheng, C.: The changing nature of groundwater in the global water cycle, Science, 383, eadf0630, https://doi.org/10.1126/science.adf0630, 2024.

Lawrence, D. M., Fisher, R. A., Koven, C. D., Oleson, K. W., Swenson, S. C., Bonan, G., Collier, N.,

https://doi.org/10.5194/essd-2025-497
Preprint. Discussion started: 13 October 2025

Ghimire, B., van Kampenhout, L., Kennedy, D., Kluzek, E., Lawrence, P. J., Li, F., Li, H., Lombardozzi, D., Riley, W. J., Sacks, W. J., Shi, M., Vertenstein, M., Wieder, W. R., Xu, C., Ali, A. A., Badger, A. M., Bisht, G., van den Broeke, M., Brunke, M. A., Burns, S. P., Buzan, J., Clark, M., Craig, A., Dahlin, K., Drewniak, B., Fisher, J. B., Flanner, M., Fox, A. M., Gentine, P., Hoffman, F., Keppel-Aleks, G., Knox, R., Kumar, S., Lenaerts, J., Leung, L. R., Lipscomb, W. H., Lu, Y., Pandey, A., Pelletier, J. D., Perket, J., Randerson, J. T., Ricciuto, D. M., Sanderson, B. M., Slater, A., Subin, Z. M., Tang, J., Thomas, R. Q., Martin, M. V., and Zeng, X.: The Community Land Model version 5: description of new features, benchmarking, and impact of forcing uncertainty, J. Adv. Model. Earth Syst., 11, 4245-4287, https://doi.org/10.1029/2018ms001583, 2019.

Li, F., Kusche, J., Chao, N., Wang, Z., and Loecher, A.: Long-term (1979-present) total water storage anomalies over the global land derived by reconstructing GRACE Data, Geophys. Res. Lett., 48, e2021GL093492, https://doi.org/10.1029/2021gl093492, 2021.

Li, Q., Shi, G., Shangguan, W., Nourani, V., Li, J., Li, L., Huang, F., Zhang, Y., Wang, C., Wang, D., Qiu, J., Lu, X., and Dai, Y.: A 1 km daily soil moisture dataset over China using in situ measurement and machine learning, Earth Syst. Sci. Data, 14, 5267-5286, https://doi.org/10.5194/essd-14-5267-2022, 2022.

Link, A., El-Hokayem, L., Usman, M., Conrad, C., Reinecke, R., Berger, M., Wada, Y., Coroama, V., and Finkbeiner, M.: Groundwater-dependent ecosystems at risk - global hotspot analysis and implications, Environ. Res. Lett., 18, 094026, https://doi.org/10.1088/1748-9326/acea97, 2023.

Liu, Y., Shan, F., Yue, H., Wang, X., and Fan, Y.: Global analysis of the correlation and propagation among meteorological, agricultural, surface water, and groundwater droughts, J. Environ. Manage., 333, 117460, https://doi.org/10.1016/j.jenvman.2023.117460, 2023.

McNally, A., Jacob, J., Arsenault, K., Slinski, K., Sarmiento, D. P., Hoell, A., Pervez, S., Rowland, J., Budde, M., Kumar, S., Peters-Lidard, C., and Verdin, J. P.: A Central Asia hydrologic monitoring dataset for food and water security applications in Afghanistan, Earth Syst. Sci. Data, 14, 3115-3135, https://doi.org/10.5194/essd-14-3115-2022, 2022.

Middleton, N. and Thomas, D.: World atlas of desertification, Oxford University Press, United Kingdom1997.

Munoz-Sabater, J., Dutra, E., Agusti-Panareda, A., Albergel, C., Arduini, G., Balsamo, G., Boussetta, S., Choulga, M., Harrigan, S., Hersbach, H., Martens, B., Miralles, D. G., Piles, M., Rodriguez-Fernandez, N. J., Zsoter, E., Buontempo, C., and Thepaut, J.-N.: ERA5-Land: a state-of-the-art global reanalysis dataset for land applications, Earth Syst. Sci. Data, 13, 4349-4383, https://doi.org/10.5194/essd-13-4349-2021, 2021.

Ombadi, M., Risser, M. D., Rhoades, A. M., and Varadharajan, C.: A warming-induced reduction in snow fraction amplifies rainfall extremes, Nature, 619, 305-310, https://doi.org/10.1038/s41586-023-06092-7, 2023.

Peng, Q., Wang, R., Jiang, Y., Li, C., and Guo, W.: The change of hydrological variables and its effects on vegetation in Central Asia, Theor. Appl. Climatol., 146, 741-753, https://doi.org/10.1007/s00704-021-03730-w, 2021.

Pinzon, J. E. and Tucker, C. J.: A non-stationary 1981-2012 AVHRR NDVI time series, Remote Sens., 6, 6929-6960, https://doi.org/10.3390/rs6086929, 2014.

Pokhrel, Y., Felfelani, F., Satoh, Y., Boulange, J., Burek, P., Gaedeke, A., Gerten, D., Gosling, S. N.,

https://doi.org/10.5194/essd-2025-497
Preprint. Discussion started: 13 October 2025

Grillakis, M., Gudmundsson, L., Hanasaki, N., Kim, H., Koutroulis, A., Liu, J., Papadimitriou, L., Schewe, J., Mueller Schmied, H., Stacke, T., Telteu, C.-E., Thiery, W., Veldkamp, T., Zhao, F., and Wada, Y.: Global terrestrial water storage and drought severity under climate change, Nat. Clim. Change, 11, 226-233, https://doi.org/10.1038/s41558-020-00972-w, 2021.

Prein, A. F. and Heymsfield, A. J.: Increased melting level height impacts surface precipitation phase and intensity, Nat. Clim. Change, 10, 771-776, https://doi.org/10.1038/s41558-020-0825-x, 2020.

Rodell, M. and Famiglietti, J. S.: An analysis of terrestrial water storage variations in Illinois with implications for the Gravity Recovery and Climate Experiment (GRACE), Water Resour. Res., 37, 1327-1339, https://doi.org/10.1029/2000wr900306, 2001.

Rodell, M. and Famiglietti, J. S.: The potential for satellite-based monitoring of groundwater storage changes using GRACE: the High Plains aquifer, Central US, J. Hydrol., 263, 245-256, https://doi.org/10.1016/s0022-1694(02)00060-4, 2002.

Rodell, M., Velicogna, I., and Famiglietti, J. S.: Satellite-based estimates of groundwater depletion in India, Nature, 460, 999-1002, https://doi.org/10.1038/nature08238, 2009.

Rodell, M., Chao, B. F., Au, A. Y., Kimball, J. S., and McDonald, K. C.: Global biomass variation and its geodynamic effects: 1982-98, Earth Interact, 9, 1–19, https://doi.org/10.1175/ei126.1, 2005.

Rodell, M., Houser, P. R., Jambor, U., Gottschalck, J., Mitchell, K., Meng, C. J., Arsenault, K., Cosgrove, B., Radakovich, J., Bosilovich, M., Entin, J. K., Walker, J. P., Lohmann, D., and Toll, D.: The global land data assimilation system, Bull. Am. Meteorol. Soc., 85, 381-394, https://doi.org/10.1175/bams-85-3-381, 2004.

Rohde, M. M., Albano, C. M., Huggins, X., Klausmeyer, K. R., Morton, C., Sharman, A., Zaveri, E., Saito, L., Freed, Z., Howard, J. K., Job, N., Richter, H., Toderich, K., Rodella, A.-S., Gleeson, T., Huntington, J., Chandanpurkar, H. A., Purdy, A. J., Famiglietti, J. S., Singer, M. B., Roberts, D. A., Caylor, K., and Stella, J. C.: Groundwater-dependent ecosystem map exposes global dryland protection needs, Nature, 632, 101-107, https://doi.org/10.1038/s41586-024-07702-8, 2024.

Schenk, H. J. and Jackson, R. B.: Mapping the global distribution of deep roots in relation to climate and soil characteristics, Geoderma, 126, 129-140, https://doi.org/10.1016/j.geoderma.2004.11.018, 2005.

Schmied, H. M., Trautmann, T., Ackermann, S., Caceres, D., Floerke, M., Gerdener, H., Kynast, E., Peiris, T. A., Schiebener, L., Schumacher, M., and Doell, P.: The global water resources and use model WaterGAP v2.2e: description and evaluation of modifications and new features, Geosci. Model Dev., 17, 8817-8852, https://doi.org/10.5194/gmd-17-8817-2024, 2024.

Shangguan, Y., Min, X., and Shi, Z.: Inter-comparison and integration of different soil moisture downscaling methods over the Qinghai-Tibet Plateau, J. Hydrol., 617, 129014, https://doi.org/10.1016/j.jhydrol.2022.129014, 2023.

Siebert, S., Burke, J., Faures, J. M., Frenken, K., Hoogeveen, J., Doell, P., and Portmann, F. T.: Groundwater use for irrigation - a global inventory, Hydrol. Earth Syst. Sci., 14, 1863-1880, https://doi.org/10.5194/hess-14-1863-2010, 2010.

Su, B., Xiao, C., Chen, D., Huang, Y., Che, Y., Zhao, H., Zou, M., Guo, R., Wang, X., Li, X., Guo, W., Liu, S., and Yao, T.: Glacier change in China over past decades: spatiotemporal patterns and influencing factors, Earth Sci. Rev., 226, 103926, https://doi.org/10.1016/j.earscirev.2022.103926, 2022.

Tapley, B. D., Bettadpur, S., Watkins, M., and Reigber, C.: The gravity recovery and climate experiment: mission overview and early results, Geophys. Res. Lett., 31, L09607, https://doi.org/10.1029/2004gl019920, 2004a.

Tapley, B. D., Bettadpur, S., Ries, J. C., Thompson, P. F., and Watkins, M. M.: GRACE measurements of mass variability in the Earth system, Science, 305, 503-505, https://doi.org/10.1126/science.1099192, 2004b.

Tavella, P. and Premoli, A.: Estimating the instabilities of N clocks by measuring differences of their readings, Metrologia, 30, 479-486, https://doi.org/10.1088/0026-1394/30/5/003, 1994.

Taylor, R. G., Scanlon, B., Doell, P., Rodell, M., van Beek, R., Wada, Y., Longuevergne, L., Leblanc, M., Famiglietti, J. S., Edmunds, M., Konikow, L., Green, T. R., Chen, J., Taniguchi, M., Bierkens, M. F. P., MacDonald, A., Fan, Y., Maxwell, R. M., Yechieli, Y., Gurdak, J. J., Allen, D. M., Shamsudduha, M., Hiscock, K., Yeh, P. J. F., Holman, I., and Treidel, H.: Ground water and climate change, Nat. Clim. Change, 3, 322-329, https://doi.org/10.1038/nclimate1744, 2013.

Wada, Y., van Beek, L. P. H., van Kempen, C. M., Reckman, J. W. T. M., Vasak, S., and Bierkens, M. F. P.: Global depletion of groundwater resources, Geophys. Res. Lett., 37, L20402, https://doi.org/10.1029/2010gl044571, 2010.

Wang, J., Song, C., Reager, J. T., Yao, F., Famiglietti, J. S., Sheng, Y., MacDonald, G. M., Brun, F., Schmied, H. M., Marston, R. A., and Wada, Y.: Recent global decline in endorheic basin water storages, Nat. Geosci., 11, 926-932, https://doi.org/10.1038/s41561-018-0265-7, 2018.

Wang, Z., Liu, S., Qiu, J., and Mo, X.: Spatiotemporal variation of water storage in 1-m soil layer in China from 1980 to 2019, Geogr. Res., 41, 2979-2999 (in Chinese), https://doi.org/10.11821/dlyj020211166, 2022.

Wang, Z., Liu, S., & Mo, X. (2025). An improved GRACE-derived groundwater storage anomaly (igGWSA) dataset over global land with full consideration of non-groundwater components based on current new datasets [Data set]. Zenodo. https://doi.org/10.5281/zenodo.16871689

Xiang, L., Wang, H., Steffen, H., Wu, P., Jia, L., Jiang, L., and Shen, Q.: Groundwater storage changes in the Tibetan Plateau and adjacent areas revealed from GRACE satellite gravity data, Earth Planet. Sci. Lett., 449, 228-239, https://doi.org/10.1016/j.epsl.2016.06.002, 2016.

Xu, L., Chen, N., Zhang, X., Moradkhani, H., Zhang, C., and Hu, C.: In-situ and triple-collocation based evaluations of eight global root zone soil moisture products, Remote Sens. Environ., 254, 112248, https://doi.org/10.1016/j.rse.2020.112248, 2021.

Yao, F., Wang, J., Wang, C., and Cretaux, J.-F.: Constructing long-term high-frequency time series of global lake and reservoir areas using Landsat imagery, Remote Sens. Environ., 232, 111210, https://doi.org/10.1016/j.rse.2019.111210, 2019.

Yao, F., Livneh, B., Rajagopalan, B., Wang, J., Cretaux, J.-F., Wada, Y., and Berge-Nguyen, M.: Satellites reveal widespread decline in global lake water storage, Science, 380, 743-749, https://doi.org/10.1126/science.abo2812, 2023.

Zhao, K., Fang, Z., Li, J., and He, C.: Spatial-temporal variations of groundwater storage in China: a multiscale analysis based on GRACE data, Resour. Conserv. Recycl., 197, 107088, https://doi.org/10.1016/j.resconrec.2023.107088, 2023.

Zou, Y., Kuang, X., Feng, Y., Jiao, J. J., Liu, J., Wang, C., Fan, L., Wang, Q., Chen, J., Ji, F., Yao, Y., and Zheng, C.: Solid water melt dominates the increase of total groundwater storage in the Tibetan

https://doi.org/10.5194/essd-2025-497
Preprint. Discussion started: 13 October 2025

821 Plateau, Geophys. Res. Lett., 49, e2022GL100092, https://doi.org/10.1029/2022gl100092, 2022.